HSSJ (2012) 8:206–212
DOI 10.1007/s11420-012-9292-x

HOSPITAL FOR SPECIAL SURGERY

Finite Element Analysis Examining the Effects of Cam FAI on Hip Joint Mechanical Loading Using Subject-Specific Geometries During Standing and Maximum Squat

K. C. Geoffrey Ng, MASc · Gholamreza Rouhi, PhD · Mario Lamontagne, PhD · Paul E. Beaulé, MD

Received: 12 December 2011/Accepted: 22 June 2012/Published online: 7 September 2012

Abstract
Background: Cam femoroacetabular impingement (FAI) can impose elevated mechanical loading in the hip, potentially leading to an eventual mechanical failure of the joint. Since in vivo data on the pathomechanisms of FAI are limited, it is still unclear how this deformity leads to osteoarthritis.
Purpose: The purpose of this study was to examine the effects of cam FAI on hip joint mechanical loading using finite element analysis, by incorporating subject-specific geometries, kinematics, and kinetics.
Questions: The research objectives were to address and determine: (1) if hips with cam FAI demonstrate higher maximum shear stresses, in comparison with control hips; (2) the magnitude of the peak maximum shear stresses; and (3) the locations of the peak maximum shear stresses.
Methods: Using finite element analysis, two patient models were control-matched and simulated during quasi-static positions from standing to squatting. Intersegmental hip forces, from a previous study, were applied to the subject-specific hip geometries, segmented from CT data, to evaluate the maximum shear stresses on the acetabular cartilage and underlying bone.
Results: Peak maximum shear stresses were found at the anterosuperior region of the underlying bone during squatting. The peaks at the anterosuperior acetabulum were substantially higher for the patients (15.2±1.8 MPa) in comparison with the controls (4.5±0.1 MPa).
Conclusions: Peaks were not situated on the cartilage, but instead located on the underlying bone. The results correspond with the locations of initial cartilage degradation observed during surgical treatment and from MRI.
Clinical Relevance: These findings support the pathomechanism of cam FAI. Changes may originate from the underlying subchondral bone properties rather than direct shear stresses to the articular cartilage.

Keywords hip · impingement · cam femoroacetabular impingement · finite element analysis · subject-specific · finite element model

The investigation was performed at the University of Ottawa, Human Movement Biomechanics Laboratory.

K. C. G. Ng, MASc · M. Lamontagne, PhD
Department of Mechanical Engineering,
University of Ottawa, Ottawa, ON, Canada

G. Rouhi, PhD
Department of Biomedical Engineering,
Amirkabir University of Technology, Tehran, Iran

M. Lamontagne, PhD (✉)
School of Human Kinetics,
University of Ottawa, Ottawa, ON K1N 6N5, Canada
e-mail: mlamon@uottawa.ca

P. E. Beaulé, MD
Division of Orthopaedic Surgery,
University of Ottawa, Ottawa, ON, Canada

Introduction

Pathological hip deformities leading to mechanical joint failures constitute a large proportion of ongoing challenges in orthopedics. Cam femoroacetabular impingement (FAI) has been identified as one such recurring geometric deformity of the femoral head [22, 34], characterized by an enlarged, aspherical femoral head–neck junction and described as a pathomechanical failure process of the hip [27]. The presence of the cam deformity introduces a substantial risk of hip pain and early osteoarthritis (OA), and it was not until the last decade that a closer assimilation was identified between cam FAI and hip degeneration, particularly in younger adults [15, 16, 18]. The impingement occurs

when the anterosuperior aspect of the femoral head is in direct interference with the acetabulum during large and combined motions in hip flexion and rotation [10, 40], as well as during squatting [9, 26]. Patients with a more severe and larger cam deformity, as defined by a higher alpha angle [6, 35, 41], can be more susceptible to anterosuperior cartilage and labral lesions [6, 7].

Although early intervention of cam FAI can decrease the risk of OA [27], detection protocols and methods to recognize the morphology remain to be an ongoing challenge [15, 28]. Moreover, knowing that the subchondral bone plays a predominant mechanical role in the initiation of cartilage degeneration [12, 36, 37], it is imperative to understand how stresses due to cam FAI are transferred directly to the articulating cartilage or are distributed to the underlying surfaces. Previous studies in literature have focused on radiographic indications, corrective surgical methods, follow-up data, and comprehensive literature reviews; however, very few studies have reconstructed the hip joint using computational modeling methods to examine the mechanical stresses due to cam FAI. To our knowledge, no study has integrated clinical subject-specific data to determine the mechanical stimuli within the impinging hip to better understand its pathomechanisms.

The purpose of this study was to examine the effects of cam FAI on hip joint mechanical loading using finite element analysis (FEA) and incorporating subject-specific geometries, kinematics, and kinetics. The mechanical stimuli magnitudes and regions can be better characterized using a more complete, subject-specific hip model [1, 44]. As a comparative study, it was hypothesized that hips with cam FAI would demonstrate a higher level of mechanical stresses, in comparison with healthy control hips. The hypothesis would further justify if mechanical stresses are higher during an activity requiring higher combined hip motions (e.g., maximal squat depth [26]) in comparison with an upright standing position and with healthy control hips. The research objectives were to address and determine: (1) if hips with cam FAI would demonstrate higher maximum shear stresses during a squatting position, in comparison with control hips performing the same task; (2) the magnitude of the peak maximum shear stresses; and (3) the locations of the peak maximum shear stresses.

Materials and Methods

The reconstruction and simulation of each finite element model (FEM) required the inputs from subject-specific motion analyses and hip joint geometries. The subject-specific kinematics and kinetics data provided the hip joint reaction forces for the squatting task, and the hip joint geometries were reconstructed from the subject-specific CT images for the FEA.

Net hip joint reaction forces of cam FAI and control participants were acquired from a previous study that compared the effects of cam FAI on pelvic hip motions and forces [26]. Two patients diagnosed with unilateral cam type FAI and two control participants were selected from the initial study for this FEA. The selected FAI participants were both male and clinically assessed to have severe cam FAI, with alpha angles greater than 65° [6, 35]. The control participants were matched with the patients by gender, body mass index, and relative physical activity level, as seen in Table 1. Exclusions of the participants included evidence of OA, joint space narrowing, previous lower limb surgeries, or serious lower limb injuries. From Lamontagne et al.'s [26] study, the participants were asked to perform a dynamic squat, squatting down to a maximal depth and then returning to an upright standing position while maintaining heel contact with the ground throughout the cycle. The intersegmental hip forces were calculated using inverse dynamics, from the subject-specific kinematics and kinetics data. The 3D kinematics of the squat motions were recorded using seven motion capture cameras (Vicon MX-13, Vicon, Oxford, UK) and retroreflective markers placed on each participant's anatomical landmarks [24], while the 3D kinetics were recorded using fixed force plates (AMTI OR6-6-2000, AMTI, Watertown, MA, USA).

To construct subject-specific geometries representative of each participant's hip joint, the proximal femur and the pelvis of each participant's pelvic CT radiographs were manually segmented into 3D models using modeling and segmentation software (3D-Doctor 4.0, Able Software Corp., Lexington, MA, USA). The affected side for both patients was coincidentally the left hip; therefore, only the left hip model of each participant was segmented and matched. The CT slices in the axial view were calibrated with a thickness of 1.25 mm, thin enough to account for the complexities of the innominate structures [33]. The two segmented patient and two control-matched assemblies were then resurfaced using computer-aided design software (SolidWorks, Dassault Systèmes, Concord, MA, USA) to eliminate geometric artifacts and reduce the number of surface polygons. Larger resurfaced edges were integrated onto the smoothed contour, therefore constructing a model that required less finite elements per surface and shorter computation time [4, 39]. Alpha and center-edge (CE) angles of the resurfaced femur and pelvis models, respectively, were verified with each participant's CT images to ascertain the accuracy of the resurfacing procedure.

To form the cartilage layer, an offset method was used to extrude the surfaces of the acetabulum onto the femoral head (Fig. 1). The concavity of the acetabulum did not match the curvatures of the femoral head; thus, the resultant cartilage layer was variable in thickness. The thickness of the layer was marginally reduced towards an ellipsoidal curvature to provide sufficient joint space and prevent any interference between the contact surfaces of the femur and the acetabulum [38]. The cartilage was extruded past the periphery of the acetabular rim, thus representative of tissue at the lateral labral region. The midpoint of this layer was taken as the line separating the acetabular cartilage with the femoral head cartilage. The region of the cartilage layer at the acetabular fossa was removed; thus, the acetabular cartilage was only represented by the surfaces of the lunate and the acetabular

Table 1 Participant list and clinical assessment of each cam FAI patient (P) and control (C)

Subject	Affected leg	Gender	Age (years)	Weight (kg)	Height (cm)	BMI (kg/m^2)	Alpha angle (°)	Clinical assessment
P1	Left	Male	44	72.7	177.7	23.0	83 axial	Severe cam FAI
P2	Left	Male	29	74.9	182	22.6	73 axial 83 radial	Severe cam FAI
C1	Left	Male	54	67.4	169	23.6	42 axial	Control
C2	Left	Male	36	67.9	163.5	25.4	45 axial	Control

dome. No patient or control participant showed any indications of OA or cartilage delamination; therefore, surface discrepancies were neglected, and the cartilage was modeled as a smooth layer.

The resurfaced solid models were imported to the FEA software (ANSYS, Canonsburg, PA, USA) for simulation. All the components were meshed with tetrahedral SOLID187 elements—a 3D, higher-order, ten-node element well suited for complex objects and irregular meshes [30]. The bone geometries were modeled as linear elastic orthotropic materials (elastic moduli, E_1=11.6 GPa, E_2=12.2 GPa, E_3=19.9 GPa; shear moduli, G_{12}=4.0 GPa, G_{13}=5.0 GPa, G_{23}=5.4 GPa; and Poisson's ratios, ν_{12}=0.42, $\nu_{13}=\nu_{23}$=0.23 [11]) as opposed to a cortical–trabecular assembly [9, 38] or a cortical-only model [1, 2]. The orthotropic bone FEMs accounted for both the cortical and trabecular structures, thus eliminating the need to separately segment a trabecular component and alleviate the overuse of finite elements and computational memory. The cartilage layers were modeled as a linear elastic isotropic material (E=12 MPa; ν=0.45 [9]). The biphasic and viscoelastic properties of cartilage were not considered since the FEA involved noncyclic loads [5, 31].

The subject-specific intersegmental hip forces [26] were applied through the femoral head of the hip joint center of each assembly, for two quasi-static loading scenarios: (1) stance and (2) maximum force endured during the impinged squat (Fig. 2). Using the subject-specific kinematics data, the femur was oriented with respect to the pelvis for each of the two loading scenarios. No muscle vectors or soft tissue approximations were accounted for in the hip joint assembly; therefore, the joint reactions were justified as an applied force through the actual hip joint center [1, 2, 9]. Boundary conditions were fixed at the proximal sectioned plane of the ilium and distal sectioned plane of the femur, due to the slicing of the CT range, and an additional fixed support was applied to the pubis [2]. Knowing that cartilage is mostly under shear stresses [20, 27, 31] and that von Mises stresses may underestimate results for quasi-brittle bone FEMs, maximum shear stress (MSS) was determined to observe the adverse loading conditions, by taking into account the principal stress components to determine the resultant shear stresses. For all patient and control FEMs, the MSS distributions and peak magnitudes were examined on the acetabular cartilage (cart) and on the underlying surfaces on the acetabular dome (bone).

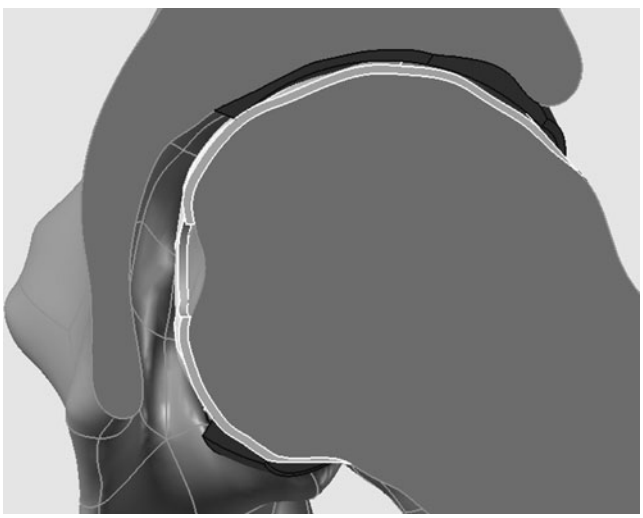

Fig. 1. Cross-sectional frontal view of the left hip joint assembly indicating the variable thicknesses of the acetabular cartilage (*black*) and the femoral cartilage (*light grey*)

Results

After segmentation and resurfacing, the alpha and CE angles of the FEMs correlated well with the original CT data (R_α^2=0.999, R_{CE}^2=0.996). To ensure that the number and size of elements were sensitive, a convergence analysis was conducted for the meshing method. The mesh was refined at acetabular regions that initially experienced the peak levels of MSS concentrations. In subsequent iterations for each FEM, the elements were reduced in size, thus increasing the number of elements until the resultant MSS output became consistent and reached convergence.

The hips with cam FAI demonstrated higher peak MSS values during the squatting task, in comparison with the control hips. For the two patient FEMs, changes in MSS on the cartilage layer were marginal between standing and squatting, for patient 1 ($P1_{cart,stand}$=3.7, $P1_{cart,squat}$=3.9 MPa) and patient 2 ($P2_{cart,stand}$=4.1, $P2_{cart,squat}$=3.3 MPa). However, substantially higher MSS magnitudes were found behind the cartilage, from standing to squatting, for both patient 1 ($P1_{bone,stand}$=3.4, $P1_{bone,squat}$=13.4 MPa) and patient 2 ($P2_{bone,stand}$=3.6, $P2_{bone,squat}$=16.9 MPa), localized at the anterosuperior acetabulum during the squatting position. For the control FEMs, MSS magnitudes were found to be uniformly distributed on the cartilage from standing to squatting, for control 1 ($C1_{cart,stand}$=3.5, $C1_{cart,squat}$=4.0 MPa) and control 2 ($C2_{cart,stand}$=2.0, $C2_{cart,squat}$=3.1 MPa); similarly, on the underlying acetabulum for both control FEMs from

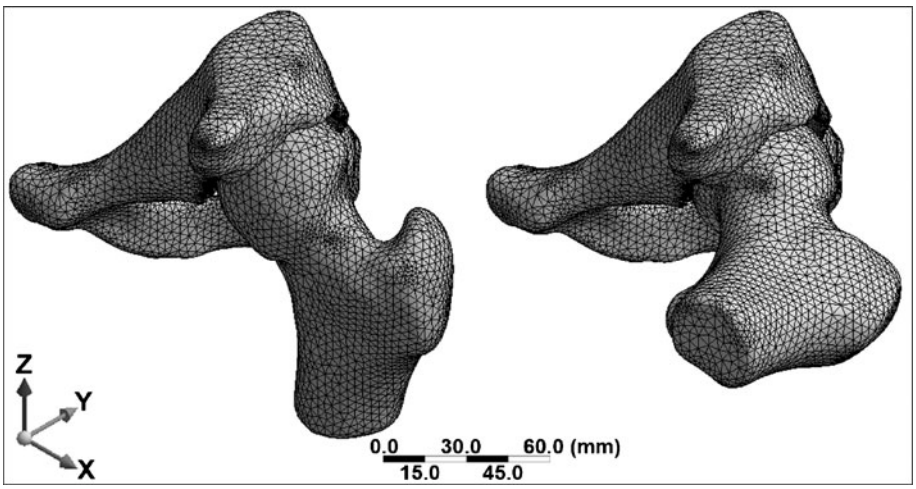

Fig. 2. Isometric view of hip joint assembly during the standing position (*left*) and the squatting position (*right*). Using the subject-specific kinematics data, the femur was oriented with respect to the pelvis according to the squat interval. The *X*–*Y*–*Z*-axis corresponds with the left hip's lateral–posterior–superior directions

standing to squatting ($C1_{bone,stand}$=3.5, $C1_{bone,squat}$= 4.5 MPa; $C2_{bone,stand}$=3.2, $C2_{bone,squat}$=4.4 MPa).

The patient models revealed isolated MSS concentrations as opposed to the control models, which exhibited more well-distributed MSS. As the participants performed the squat, the peak levels displaced from the superolateral to the anterolateral regions, though very little changes in magnitudes of MSS were noticed on the cartilage layer. During the squatting position for all participants, the highest MSS peaks were found at the anterosuperior regions of the underlying bone, with secondary MSS concentrations located at the posteroinferior acetabulum, representative of the contrecoup lesion [15]. It was noticed that the highest peak MSS among the participants ($P2_{bone,squat}$=16.9 MPa) was experienced by the patient with the more severe impingement (combined alpha angles of 74° and 83° in the axial and radial planes, respectively). Figure 3 summarizes the MSS distributions on the cartilage and underlying acetabulum during the squatting position for each participant.

At the depth of squat, the cam deformity of the femoral head–neck junction was at the highest point of contact within the labral–chondral junction of the acetabulum, when the joint was at its most impinged state. The cam deformity caused a reduction in clearance within the socket, causing a distortion of the elastic members from an unstressed state. Table 2 summarizes the peak MSS found on the cartilage and acetabulum for each hip model.

Discussion

The FEMs from this study were reconstructed from subject-specific CT data and incorporated subject-specific intersegmental hip forces, which was a different approach from previous works on cam FAI. The inclusion of a pelvis model in this study provided a constraint for the acetabular cartilage and physiological rigidity to permit proper representation of mechanical stress distributions on the acetabulum. Several past studies have questioned the implementation of subject-specific geometries, arguing that the approach requires a considerable amount of manual correction and imposes convergence issues. Thus, the subject-specific approach has often been avoided in many previous studies involving hip modeling. However, not only do subject-specific geometries provide a more realistic representation but also the simulations can yield results to be in better agreement with experimental data [2, 3]. It was interesting to note that minimal convergence issues were encountered in our FEA. The smoothed models reduced the number of finite elements and computation time without compromising the accuracy of the geometries, as confirmed by the alpha and CE angles with the original CT images.

A separate material property for the labrum was not considered in our quasi-static analysis. Although the inclusion of a labrum in hip FEMs remains elusive [2, 25], it would be beneficial in future studies to understand the residual physiological effect of the labral seal for this pathological hip condition [13, 14, 19]. Moreover, the use of intersegmental hip forces from inverse dynamics estimated the reaction forces acting through the joint. The reaction forces provided valuable approximations of the net hip joint forces and moments, but were underestimations of the in vivo contact forces acting at the hip. The incorporation of dynamic loading and nonlinear rotation should be further addressed to understand the effect of impact loading of the cam lesion with the labral regions during a subject-specific dynamic squat motion. Future research involving the inclusion of individual muscles and hip contact forces, under dynamic loading, could better represent the physiological reactions and resultant hip contact stresses [8, 29, 32].

Resultant MSS magnitudes were much higher for the patient FEMs during squatting, when the hip joint was at its most impinged state. As expected, impingement was not exposed during the standing position for both patient and control groups [9, 26]. Unlike previous studies where the evaluation of the acetabulum was

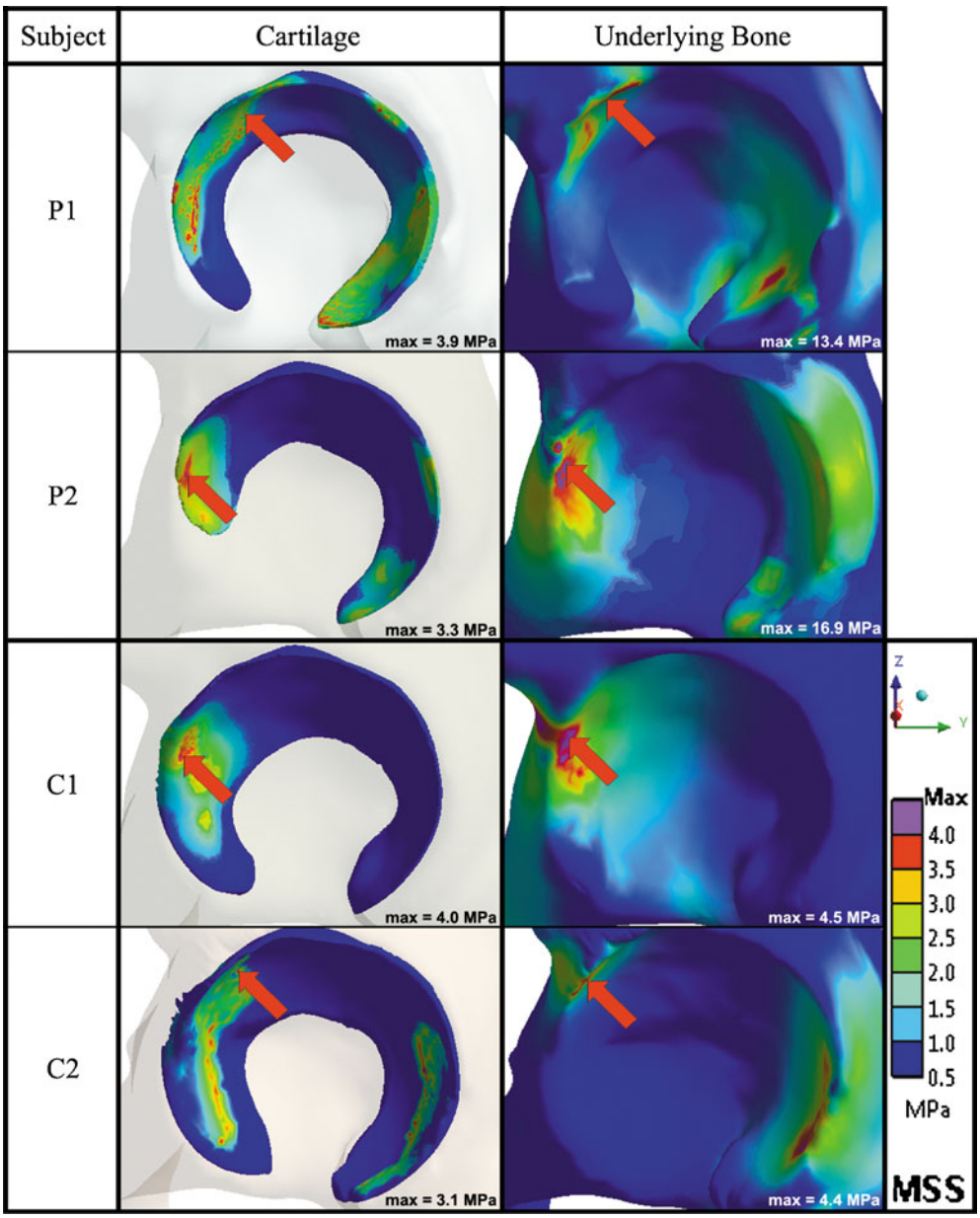

Fig. 3. Summary of the maximum shear stress (MSS) distributions on the acetabular cartilage and underlying bone of the acetabulum during the squatting position for each participant's left hip in the sagittal plane. The *red arrow* denotes the location of the peak MSS

neglected [1, 2, 9, 38], the peak stresses in our FEA were not situated on the cartilage, but instead were located on the underlying bone of the acetabulum [37, 43]. These peaks could have been due to the lower

Table 2 Summary of peak maximum shear stress (MSS) magnitudes on the acetabular cartilage and underlying bone of the acetabulum

Subject	Alpha angle of FEM (°)*	Standing position		Squatting position	
		Acetabular cartilage (MPa)	Underlying bone (MPa)	Acetabular cartilage (MPa)	Underlying bone (MPa)
P1	84	3.7	3.4	3.9	13.4
P2	74 (axial), 83 (radial)	4.1	3.6	3.3	16.9
C1	41	3.5	3.5	4.0	4.5
C2	45	2.0	3.2	3.1	4.4

*Alpha angles measured from segmented FEMs demonstrated marginal differences from angles measured directly from original CT data

elastic modulus of the cartilage layer. Since cartilage was less stiff in comparison with the adjacent underlying bone, it was possible that it transferred the load and amplified the stresses reaching the subchondral bone. The change in material stiffness and variable thicknesses could have also affected the different distributions and the locations of the resultant peak stresses between the cartilage and the underlying bone. Based on our results, it is speculated that the amplification of high MSS in hips with cam FAI may increase the rate of remodeling in the subchondral bone, thus stiffening the bone plate and creating an onset for OA [12, 36, 37, 43].

Our resultant peak stresses were similar to a recent study on cam FAI by Chegini et al. [9], where an idealized parametric ball-and-socket model was implemented to examine a similar stand-to-sit motion. However, Chegini et al. evaluated the von Mises stresses of the cartilage, a more conservative failure criterion for ductile materials, without considering the principal stress components on the underlying bone. It should be noted that the cam deformities of our patients were more severe than Chegini et al.'s parametric FEM, which simulated an upper alpha angle of 80° that produced contact pressures on the acetabular cartilage in the range of 12.84 MPa (alpha=80°, CE=30°) and 16.51 MPa (alpha=80°, CE=40°) [9]. Since joint loading was taken as a proportion of body weight in their study, the hip forces were not associated with the constructed FEM. Thus, subject-specific joint loading and geometries were not included in their FEA.

The regions of peak MSS determined from our FEA, located at the anterosuperior acetabulum, corresponded to known areas of acetabular rim damage noted at the time of surgical intervention and on MRI [6, 7, 41], where delamination of the acetabular cartilage was attributed to shearing from the subchondral bone [6]. Secondary MSS concentrations, located at the posteroinferior acetabulum, may have been due to the alignment of the intersegmental hip forces during squatting, which were oriented by the vectors of the femoral axis. Interestingly, lesions at the posteroinferior acetabulum have been described as secondary to the chronic leverage of the femoral head within the acetabulum [15]. The discrepancies between each participant and both comparison groups were due to the subject-specific inputs and could be consistent with the known variability of joint kinematics, emphasizing the need for more precise models to study the pathomechanisms of FAI.

Although the results indicated that peak MSS could reach the underlying bone, a separate subchondral bone model was not included in the hip joint assembly at the time of the study. The difference in MSS between the cartilage and the underlying bone was evident among the two comparison groups; however, the subsequent step to include the subchondral bone would yield an improvement to the model. In addition, the rate of bone remodeling in the subchondral bone was not investigated and was beyond the scope of this study. Further research would be needed to understand and quantify a mechanical stimulus that would regulate the subchondral bone's density. As a mechanical stimulus, it has been documented that by increasing strain energy density, there would be an increase in bone apparent density due to the bone remodeling process [21, 42]. In this case, viscoelastic cartilage models under iterative loading should be considered in the future [17, 23], manipulating the rate of loading and to understand subject-specific thresholds that govern bone remodeling.

This study provided a modeling perspective of cam FAI and integrated more subject-specific data to further understand the pathomechanism with mechanical stimuli corresponding to the known areas of acetabular cartilage damage. The elevated levels of mechanical stimuli on the underlying bone, in the presence of a cam lesion, emphasize the need to further understand the intricacy of the morphology and determine if joint degeneration may be due to the changes in local mechanical properties of the subchondral bone.

Acknowledgments The authors wish to thank Matthew J. Kennedy, research associate of the Human Movement Biomechanics Laboratory at the University of Ottawa; Andrew D. Speirs MD, research engineer of the Division of Orthopaedic Surgery at the Ottawa Hospital; and Michel R. Labrosse, director of the Ottawa-Carleton Institute for Biomedical Engineering, for their research contributions and insight. The authors wish to also acknowledge the funding contributions from the Hans K. Uhthoff Graduate Fellowship Award and the Canadian Institutes of Health Research.

Disclosures One or more authors (ML and PB) have received funding from the Canadian Institutes of Health Research. One and more of the authors (PB) has or may receive payments or benefits from a commercial entity (Wright Medical Technology, Medacta) that may be perceived as a potential conflict of interest.

Each author certifies that his or her institution has approved the reporting of this study, and that all investigations were conducted in conformity with ethical principles of research.

References

1. Anderson AE, Ellis BJ, Maas SA, Peters CL, Weiss JA. Validation of finite element predictions of cartilage contact pressure in the human hip joint. J Biomech Eng. 2008;130(5):051008.
2. Anderson AE, Ellis BJ, Maas SA, Weiss JA. Effects of idealized joint geometry on finite element predictions of cartilage contact stresses in the hip. J Biomech. 2010;43(7):1351–7.
3. Arbabi E, Boulic R, Thalmann D. Fast collision detection methods for joint surfaces. J Biomech. 2009;42(2):91–9.
4. Aritan S, Dabnichki P, Bartlett R. Program for generation of three-dimensional finite element mesh from magnetic resonance imaging scans of human limbs. Med Eng Phys. 1997;19(8):681–9.
5. Ateshian GA, Ellis BJ, Weiss JA. Equivalence between short-time biphasic and incompressible elastic material responses. J Biomech Eng. 2007;129(3):405–12.
6. Beaule PE, Zaragoza E, Motamedi K, Copelan N, Dorey FJ. Three-dimensional computed tomography of the hip in the assessment of femoroacetabular impingement. J Orthop Res. 2005;23(6):1286–92.
7. Beck M, Kalhor M, Leunig M, Ganz R. Hip morphology influences the pattern of damage to the acetabular cartilage: femoroacetabular impingement as a cause of early osteoarthritis of the hip. J Bone Joint Surg. 2005;87(7):1012–8.

8. Buchanan TS, Lloyd DG, Manal K, Besier TF. Estimation of muscle forces and joint moments using a forward-inverse dynamics model. Med Sci Sports Exerc. 2005;37(11):1911–6.
9. Chegini S, Beck M, Ferguson SJ. The effects of impingement and dysplasia on stress distributions in the hip joint during sitting and walking: a finite element analysis. J Orthop Res. 2009;27(2):195–201.
10. Clohisy JC, McClure JT. Treatment of anterior femoroacetabular impingement with combined hip arthroscopy and limited anterior decompression. Iowa Orthop J. 2005;25:164–71.
11. Couteau B, Hobatho MC, Darmana R, Brignola JC, Arlaud JY. Finite element modelling of the vibrational behaviour of the human femur using CT-based individualized geometrical and material properties. J Biomech. 1998;31(4):383–6.
12. Day JS, Van Der Linden JC, Bank RA, Ding M, Hvid I, Sumner DR, et al. Adaptation of subchondral bone in osteoarthritis. Biorheology. 2004;41(3–4):359–68.
13. Ferguson SJ, Bryant JT, Ganz R, Ito K. The acetabular labrum seal: a poroelastic finite element model. Clin Biomech (Bristol, Avon). 2000;15(6):463–8.
14. Ferguson SJ, Bryant JT, Ganz R, Ito K. The influence of the acetabular labrum on hip joint cartilage consolidation: a poroelastic finite element model. J Biomech. 2000;33 (8):953–60.
15. Ganz R, Leunig M, Leunig-Ganz K, Harris WH. The etiology of osteoarthritis of the hip: an integrated mechanical concept. Clin Orthop Relat Res. 2008;466(2):264–72.
16. Ganz R, Parvizi J, Beck M, Leunig M, Notzli H, Siebenrock KA. Femoroacetabular impingement: a cause for osteoarthritis of the hip. Clin Orthop Relat Res. 2003;417:112–20.
17. Gilbert JL. Complexity in modeling of residual stresses and strains during polymerization of bone cement: effects of conversion, constraint, heat transfer, and viscoelastic property changes. J Biomed Mater Res A. 2006;79(4):999–1014.
18. Gosvig KK, Jacobsen S, Sonne-Holm S, Gebuhr P. The prevalence of cam-type deformity of the hip joint: A survey of 4151 subjects of the copenhagen osteoarthritis study. Acta Radiologica. 2008;49 (4):436–41.
19. Henak CR, Ellis BJ, Harris MD, Anderson AE, Peters CL, Weiss JA. Role of the acetabular labrum in load support across the hip joint. J Biomech. 2011;44(12):2201–6.
20. Hlavacek M. The thixotropic effect of the synovial fluid in squeeze-film lubrication of the human hip joint. Biorheology. 2001;38(4):319–34.
21. Huiskes R, Ruimerman R, van Lenthe GH, Janssen JD. Effects of mechanical forces on maintenance and adaptation of form in trabecular bone. Nature. 2000;405(6787):704–6.
22. Ito K, Minka MA, 2nd, Leunig M, Werlen S, Ganz R. Femoroacetabular impingement and the cam-effect. A MRI-based quantitative anatomical study of the femoral head-neck offset. J Bone Joint Surg. 2001;83(2):171–6.
23. Johnson GA, Tramaglini DM, Levine RE, Ohno K, Choi NY, Woo SL. Tensile and viscoelastic properties of human patellar tendon. J Orthop Res. 1994;12(6):796–803.
24. Kadaba MP, Ramakrishnan HK, Wootten ME. Measurement of lower extremity kinematics during level walking. J Orthop Res. 1990;8(3):383–92.
25. Konrath GA, Hamel AJ, Olson SA, Bay B, Sharkey NA. The role of the acetabular labrum and the transverse acetabular ligament in load transmission in the hip. J Bone Joint Surg Am. 1998;80(12):1781–8.
26. Lamontagne M, Kennedy MJ, Beaule PE. The effect of cam FAI on hip and pelvic motion during maximum squat. Clin Orthop Relat Res. 2009;467(3):645–50.
27. Leunig M, Beaule PE, Ganz R. The concept of femoroacetabular impingement: current status and future perspectives. Clin Orthop Relat Res. 2009;467(3):616–22.
28. Leunig M, Beck M, Dora C, Ganz R. Femoroacetabular Impingement: Etiology and Surgical Concept. Oper Tech Orthop. 2005;15:247–55.
29. Lloyd DG, Buchanan TS, Besier TF. Neuromuscular biomechanical modeling to understand knee ligament loading. Med Sci Sports Exerc. 2005;37(11):1939–47.
30. Luo Y. 3D Nearest-Nodes Finite Element Method for Solid Continuum Analysis. Adv Theor Appl Mech. 2008;1(3):131–9.
31. Macirowski T, Tepic S, Mann RW. Cartilage stresses in the human hip joint. J Biomech Eng. 1994;116(1):10–8.
32. Manal K, Gonzalez RV, Lloyd DG, Buchanan TS. A real-time EMG-driven virtual arm. Comput Biol Med. 2002;32(1):25–36.
33. Murphy MJ. The importance of computed tomography slice thickness in radiographic patient positioning for radiosurgery. Med Phys. 1999;26(2):171–5.
34. Myers SR, Eijer H, Ganz R. Anterior femoroacetabular impingement after periacetabular osteotomy. Clin Orthop Relat Res. 1999; (363):93–9.
35. Notzli HP, Wyss TF, Stoecklin CH, Schmid MR, Treiber K, Hodler J. The contour of the femoral head-neck junction as a predictor for the risk of anterior impingement. J Bone Joint Surg. 2002;84(4):556–60.
36. Radin EL, Paul IL, Tolkoff MJ. Subchondral bone changes in patients with early degenerative joint disease. Arthritis Rheum. 1970;13(4):400–5.
37. Radin EL, Rose RM. Role of subchondral bone in the initiation and progression of cartilage damage. Clin Orthop Relat Res. 1986; (213):34–40.
38. Russell ME, Shivanna KH, Grosland NM, Pedersen DR. Cartilage contact pressure elevations in dysplastic hips: a chronic overload model. J Orthop Surg Res. 2006;1:6.
39. Shaffer E, Garland M. A multiresolution representation for massive meshes. IEEE Trans Vis Comput Graph. 2005;11 (2):139–48.
40. Siebenrock KA, Wahab KH, Werlen S, Kalhor M, Leunig M, Ganz R. Abnormal extension of the femoral head epiphysis as a cause of cam impingement. Clin Orthop Relat Res. 2004;(418):54–60.
41. Tannast M, Siebenrock KA, Anderson SE. Femoroacetabular impingement: radiographic diagnosis–what the radiologist should know. AJR Am J Roentgenol. 2007;188(6):1540–52.
42. Vahdati A, Rouhi G. A model for mechanical adaptation of trabecular bone incorporating cellular accommodation and effects of microdamage and disuse. Mech Res Comm. 2009;36(3):284–293.
43. Wei HW, Sun SS, Jao SH, Yeh CR, Cheng CK. The influence of mechanical properties of subchondral plate, femoral head and neck on dynamic stress distribution of the articular cartilage. Med Eng Phys. 2005;27(4):295–304.
44. Yoshida H, Faust A, Wilckens J, Kitagawa M, Fetto J, Chao EY. Three-dimensional dynamic hip contact area and pressure distribution during activities of daily living. J Biomech. 2006;39(11):1996–2004.